The Free Internet Journal
for Organic Chemistry

Paper

Archive for
Organic Chemistry

Arkivoc **2020**, part vi, 287-298

Temperature dependent analysis of Octenidine (*N*,*N*´-(decane-1,10-diyldipyridin-1-yl-4-ylidene)dioctan-1-amine) dihydrochloride by NMR and NIR spectroscopy

David L. Mainka,[a]* Jörg Schwarz,[b] and Ulrich Girreser[b]

[a]*Institute of Pharmacy, University of Greifswald,Friedrich-Ludwig-Jahn-Str. 17, 17489 Greifswald*
[b]*Institute of Pharmacy, University of Kiel, Gutenbergstr. 76, 24118 Kiel*
Email: david-mainka@gmx.de

Received 03-02-2020 **Accepted** 05-11-2020 **Published on line** 08-24-2020

Abstract

Octenidine dihydrochloride is one of the most common active pharmaceutical incredients with a disinfectant effect on superficial wounds. In this paper we describe the mesomeric behaviour of Octenidine dihydrochloride by comparison with ^{1}H, ^{13}C and ^{15}N NMR shift data. With various NMR experiments, the possible mesomeric structures are studied and it is shown that an *E*/*Z*-isomerization plays a role, corresponding to a hindered rotation of the heteroaromatic pyridine ring. In this context, NIR spectroscopy and principal component analysis emphasize the occurrence of a modified temperature-dependent spectral behaviour of Octenidine dihydrochloride. In addition, we made a detailed study of the NMR-characteristics of Octenidine dihydrochloride using 1D- and 2D-experiments.

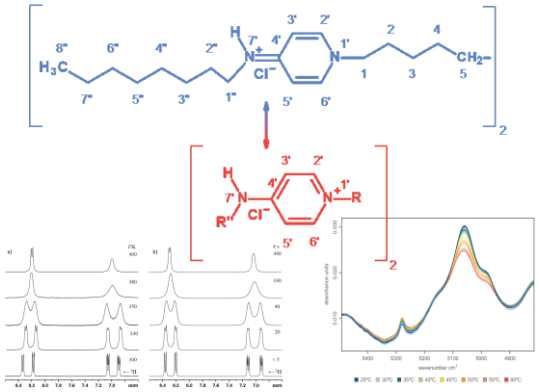

Keywords: Octenidine dihydrochloride, *E*/*Z* isomerization, NIR spectroscopy, NMR spectroscopy, nitrogen heterocycles

Introduction

The pharmaceutical drug Octenidine dihydrochloride is one of the most important disinfectant drugs for superficial wounds.[1] Its use is restricted to superficial wounds, as clarified by the manufacturer in 2011 after some adverse drug reactions in Germany with a so-called 'Rote-Hand-Brief' (warning letter after detection of adverse drug reactions).[2] In cavities or when there is a lack of drainage for the sore liquid the substance Octenidine dihydrochloride leads to necrosis of the affected tissue. When used superficially, it works excellently as a disinfectant.[3] The differences in the effects, when using Octenidine dihydrochloride, may be linked to changes in the structure. Similar necrotic effects have been reported for e.g. cetyl pyridinium chloride, a cationic quaternary ammonium structure.[4,5] If so, the description of mesomeric structures may yield an explanation for the different modes of action of this API (active pharmaceutical ingredient). Therefore, we carried out a temperature-dependent analysis of the API with NMR and NIR spectroscopy. Based on the molecular structure of Octenidine dihydrochloride the major canonical forms, shown in Scheme 1, should be discussed.

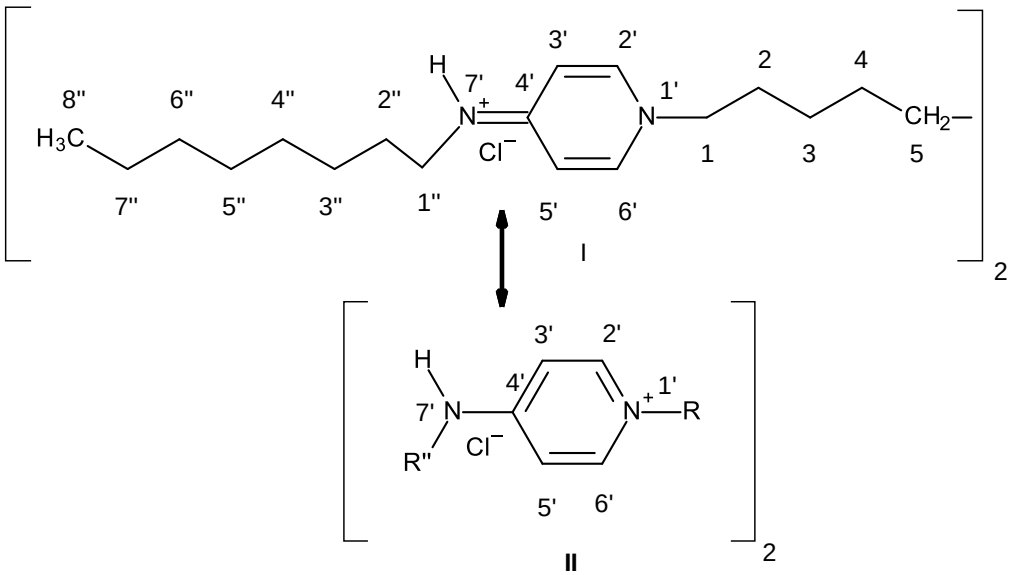

Scheme 1. Mesomeric structures **I** and **II** of Octenidine dihydrochloride.

Whereas structure **I** has a C=N-double bond as an iminium salt, the resonance structure **II** can be denominated a pyridinium ion. Therefore, the C=N-double bond has characteristics – similar to the C-N bond in the amide functional group – of a partial double bond. The remaining relevant canonical forms with the charge located at carbon atoms are given in Figure S1.

Results and Discussion

Structure elucidation and assignment of ^{1}H, ^{13}C, and ^{15}N NMR shifts

Octenidine dihydrochloride was dissolved in deuterated DMSO (dimethyl sulfoxide-d_6) and examined by conventional 1D and 2D NMR experiments. All the signals are summarized in Table 1; full spectra are given in the supporting information. Looking first at the ^{1}H NMR spectrum of this symmetric molecule with two

perpendicular mirror planes, a high frequency shifted NH signal can be identified at about 9.1 ppm as a triplet. Next to this signal four doublets of doublets in the olefinic region of the proton NMR spectrum are noticeable, corresponding to the signals in position 2', 3', 5' and 6' (shown in Figure 1 and Figure S4 and S5) in the range of 8.3 to 6.9 ppm. Clearly, the four signals can be best explained by looking at the mesomeric structure **I** in Scheme 1, the iminium isomer with chemically non-equivalent sides of the substituted dihydropyridine ring with protons in *E* and *Z* position relative to the alkyl group at the C=N double bond. Each of the signals is split by a coupling over three and one over four bonds. A first order analysis of this AGMX system explains the basic splitting of these olefinic signals.

Using a 2D NOESY experiment the protons next to the iminium proton can be assigned and also the methylene groups in the vicinity of this NH proton, thereby allowing the assignment of all the different olefinic signals. The remaining protons, i.e. all the methylene groups without a nitrogen atom in the vicinity, resonate as a broad multiplet centred around 1.25 ppm.

Table 1. ^{1}H, ^{13}C and ^{15}N NMR shifts of Octenidine dihydrochloride in DMSO-d_6

atom no	δ(^{13}C [a]) or ^{15}N[b])/ppm	δ(^{13}C) prediction/ppm		δ(^{1}H)/ppm (multiplicity, *J*/Hz, integral)[c]	further NMR spectroscopic details
		iminium ion	pyridinium ion		
1	56.69	51.5	60.9	4.11 (t, 7.1, 4 H)	H-1 long-range correlation to N-1'
2	30.22	27.8	29.0	1.74 (quint, 7.2, 4 H)	H-2 long-range correlation to N-1'
3	25.37	27.2	27.1	1.20 (m[d], 4 H)	
4	28.37	28.8	28.6	1.25 (m[d], 4 H)	
5	28.67	29.1	28.5	1.22 (m[d], 4 H)	
1'	170.5	N	N		δ_N = -211.1 ppm on the nitromethane scale; δ_N = -214.2 ppm in $CDCl_3$relative to nitromethane
2'	141.19	137.2	143.8	8.16 (dd, 7.4/1.5, 2 H)	H-2’ long-range correlation to N-1'
3'	110.26	111.8	111.1	7.05 (dd, 7.4/2.8, 2 H)	H-3' long-range correlation to N-1'
4'	156.62	151.2	154.5		
5'	105.10	111.4	111.1	6.90 (dd, 7.4/2.8, 2 H)	H-5' long-range correlation to N-1'
6'	143.57	137.2	143.8	8.35 (dd, 7.4/1.5, 2 H)	H-6' long-range correlation to N-1'
7'	109.0	N	N	9.09 (t, 5.5, 2 H)	^{1}J(N,H) = 91.4 Hz (92.8 Hz in $CDCl_3$), δ_N = -272.6 ppm on the nitromethane scale, δ_N = -268.8 ppm in $CDCl_3$
1''	42.18	50.1	43.8	3.24 (q, 6.9, 4 H)	H-1'' long-range correlation to N-7'
2''	27.90	29.6	29.7	1.56 (quint, 7.2, 4 H)	H-2'' long-range correlation to N-7'
3''	26.28	26.3	27.2	1.31 (m[d], 4 H)	

Table 1. Continued

4''	28.62[e)]	29.0	28.9	1.27 (m[d)], 4 H)
5''	28.61[e)]	29.0	29.0	1.27 (m[d)], 4 H)
6''	31.21	31.5	31.5	1.24 (m[d)], 4 H)
7''	21.98	22.8	22.8	1.24 (m[d)], 4 H)
8''	13.93	14.1	14.1	0.86 (t, 6.8, 6 H)

[a)] 100 MHz relative to the internal DMSO-d_6 signal at 39.5 ppm, [b)] 30.6 MHz relative to external nitromethane in DMSO-d_6 [c)] 400 MHz relative to internal TMS, [a-c)] for details see experimental section [d)] overlapping multiplets, refined shifts were taken from the ^{1}H,^{13}C HSQC spectrum [e)] assignment interchangeable

A refined determination of the ^{1}H chemical shifts of these methylene groups was performed by evaluation of the ^{1}H,^{13}C HSQC cross signals. This 2D technique was also used for the assignment of the ^{13}C NMR shifts, further information was gained from the ^{1}H,^{13}C HMBC measurement. All carbon signals can be assigned except for the two methylene group signals at 28.61 and 28.62 ppm (C-4'' and C-5''), here the assignment is interchangeable. Two special observations have to be explained: firstly the methyl group forms a distorted triplet due to a well-known higher order effect observable with long linear alkyl chains. The other effect needing explanation is the different line widths and thus different resolution and signals heights of the olefinic signals (Figure S4). These originate from unresolved long range couplings, the NH proton couples over five bonds with H-6' (an 'extended' W coupling) and a very weak interaction of the protons of methylene group 1 with H-3' but not with H-5' (also a ^5J coupling) was detectable using a long range H,H COSY.
An alternative possible tautomeric structure with protonation of the annular nitrogen atom, instead of the imine nitrogen, can be easily excluded by analysis of the ^{1}H,^{15}N HSQC and HMBC spectrum, as the proton at about 9.1 ppm shows coupling to the imine nitrogen atom N-7' and not to the endocyclic nitrogen atom N-1'. Moreover, the NH long range couplings confirm the assignment of the ^{15}N NMR shifts, the endocyclic nitrogen atom 1' at 170 ppm shows coupling with all four olefinic protons and the high frequency shifted methylene group at about 4.1 ppm. There is no evidence in any of the spectra for the presence for this or any other tautomer.

Predicted NMR shifts for the ^{1}H and ^{13}C nucleus were calculated using established online prediction portals based on experimental values in order to describe the structure of Octenidine dihydrochloride by the observed NMR shift values. The predictions are based either on neural networks which are trained by experimental NMR shift data[6,7] or by comparison of chemical shifts using the so-called HOSE (hierarchically ordered spherical environment) code, which is also able to encode three-dimensional structures, that means considering stereochemical information,[8,,9] which is, however, not relevant for Octenidine. Some prediction tools use both methods. The predicted shifts are obtained after generating the HOSE code of the atom under investigation and searching the chemical shift library for atoms with the same HOSE code. If several values are found they are averaged. Some of the prediction portals use both methods. The libraries contain a huge amount of experimental NMR shifts, e.g. in the case of the ^{13}C prediction portal about five hundred thousand spectra. Especially the ^{13}C prediction tool is even used to check the quality of submitted ^{13}C NMR shift data for inconsistencies by organic chemistry journals.[10]

For the two different canonical forms **I** and **II** with the positive charge located at the nitrogen atom (we named these resonance structures pyridinium and iminium ions compared to the remaining three mesomeric structures named carbenium ions 1-3, Scheme 1 and Figure S3), the predicted values are given in Tables S1

and S2. It is quite obvious from this comparison, especially when looking only at the values predicted for the atoms near the nitrogen atoms, that the ^{1}H and ^{13}C chemical shifts describe best the pyrimidinium ion, here a minimum for the standard deviation between observed and predicted shifts is observed. When estimating the charge distribution with a simple tool (HMO charge distribution within MarvinSketch), more than 40% of the charge is localized at the endocyclic nitrogen atom and the remainder is distributed nearly equally on the two *ortho* carbon positions, the carbon in *para* position and the imine nitrogen (Figure S2).

The chemical shifts of the nitrogen atoms are also in accordance with this charge distribution. Beltrame et al.[11] observed ^{15}N shift values of 159.9 and 91.5 ppm for the endocyclic and the exocyclic nitrogen atom, respectively, for protonated 4-aminopyridine, which are quite similar to the measured values of 170.5 and 109.0 ppm in Octenidine dihydrochloride, considering different standards and the necessity for re-referencing (see Table S3), the use of a solvent mixture (changing from DMSO-d_6 to $CDCl_3$ decreases the shift values up to 10 ppm,[7] the additional alkyl substituent at both nitrogen atoms in Octenidine dihydrochloride (methylation for uncharged nitrogen atoms leads to a shift of the resonance frequency to lower values up to 5 ppm,[12]) and finally the additional compounds present in solution in the 4-aminopyridine measurement, where protonation was achieved by addition of pyridinium chloride. Especially the shift of the endocyclic nitrogen atom fits also well with the shift value observed in 4-pyridone (155.1 ppm with a calculated charge HMO charge density of 0.40) and even better with the protonated form of 4-pyridone, that is the 4-hydroxypyridinium ion (175.4 ppm; HMO charge density 0.46, see Figure S4).[13] This simple approach, however, does not work similarly well for the evaluation of the shift of the exocyclic iminium-type nitrogen atom. Protonation effects on the nitrogen chemical shifts, especially also in imines, have been analysed on a theoretical level only recently[14,15] the imine nitrogen in Schiff bases, i.e. N-substituted ketimines and aldimines and also conjugated aliphatic imines,[16] resonates in the range of 320 to 340 ppm, protonation leads to a remarkable low frequency shift of up to 150 ppm to typical shift values of 200 ppm. In a special case, for intramolecular protonation of the imine function via tautomerism, a shift of the ^{15}N signal to 142 ppm for the protonated form has been observed in the solid state.[17]

Temperature dependent ^{1}H-NMR-spectra

^{1}H NMR spectra of Octenidine dihydrochloride were recorded at increasing temperatures in order to gain more insight into the dynamics of this system.[18] Figure 1 shows the expansions of the olefinic region between 300 and 400 K, whole spectra are given in the supporting information. The signals show coalescence and develop – at least partly - into two doublet structures. The spectra were simulated with some simplifications: i) mutual exchange of the protons A with G and also M with X with one exchange rate was assumed which would end up in the fast exchange region in a simple A_2X_2 system, higher order effects are thus not considered ii) the above mentioned long-range couplings were neglected, iii) the broadening of the NH triplet was also not analysed and probably originates by an inter- or intramolecular exchange process with other NH protons or the water in the sample. The simulated spectra (Figure 1b) generated using the chemical shifts from the room temperature spectrum describe the measured spectra reasonably well without achieving a perfect fit as three of the signals show a small low frequency shift with increasing temperature, one signal is high frequency shifted. Near the low-temperature limit of the solvent DMSO-d_6 at room temperature the linewidths in this viscous solvent prohibit a reliable determination of the exchange rate k ($k < 5$ s^{-1}) and the estimated values were not employed in the determination of the thermodynamic parameters. The Eyring plot of ln (k/T) versus 1/T is given in the supporting information (S35), thereby an activation enthalpy of $\Delta H^{‡}$ = 48 kJ/mol was calculated and an activation entropy of $\Delta S^{‡}$ = –76 J/(mol K) was determined in two different experiments at 300 and 400 MHz measuring frequency with an estimated error of about 10%. In a third experiment, about 5%

of D_2O was added to the DMSO-d_6 solution whereby the NH proton nearly disappeared and the two signals at about 7 ppm (H-3' and H-5') moved much closer together and formed higher order multiplets. The other two olefinic signals at 8 ppm, however, allowed the determination of the inversion barrier, affording a similar coalescence and quite similar parameters ($\Delta H^{‡}$ = 51.5 kJ/mol, $\Delta S^{‡}$ = –62 J/(mol K) in this solvent mix. This coalescence is also observable in the proton decoupled ^{13}C NMR spectra, when the carbon signals for the four olefinic methine groups broaden extremely at temperatures above 320 K, leading – in practice in diluted solutions – to a complete disappearance of these signals (spectra not shown).

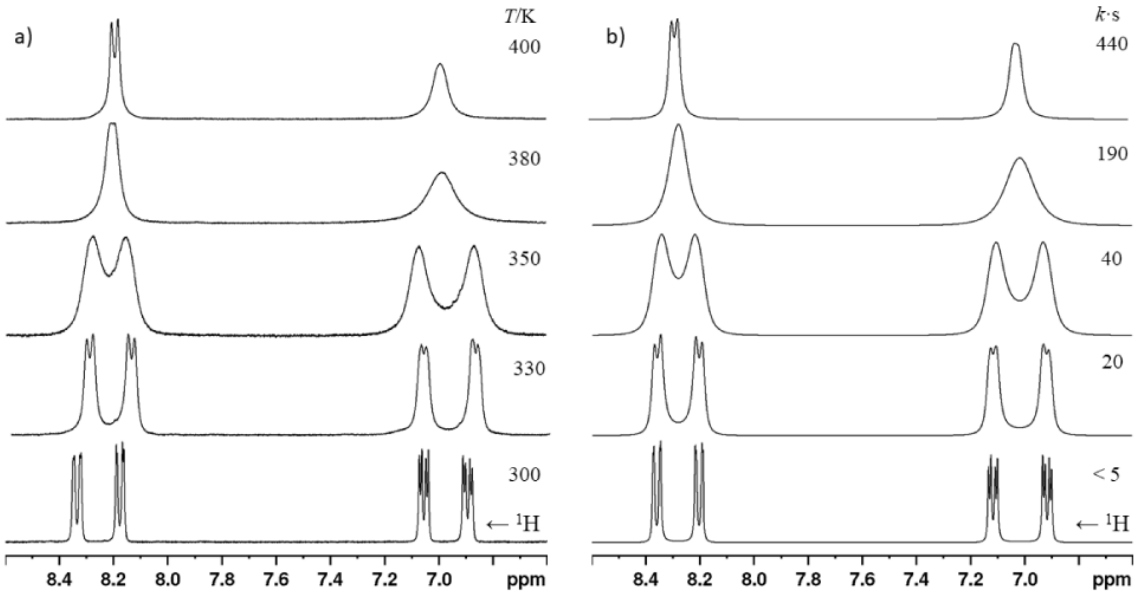

Figure 1. a) temperature dependent ^1H NMR spectra of Octenidine dihydrochloride in the range of 8.6 to 6.6 ppm from 300 to 400 Kb) simulated spectra with exchange rates.

For the barrier of *E/Z* isomerization of substituted imines, values between 65 and 100 kJ/mol are reported.[19] It is generally accepted that protonation catalyses this isomerization thus lowering the barrier. In detailed investigations by Jennings[20] and later by Johnson[21] supported by theoretical calculations on differently substituted imines, two different mechanisms for the isomerization have to be considered: i) protonation followed by rotation and ii) nucleophilic catalysis via a tetrahedral intermediate. For Octenidine dihydrochloride, both processes are conceivable, as the chloride counter anion can partake in this process ii), however, more important is the conclusion from these calculations that substituents which stabilize the positive charge by delocalization reduce the isomerization barrier by as much as 40 to 70 kJ/mol.[21]
The Eyring plot of temperature-dependent sequence of the ^1H-spectra is accessible in the supplements.

FT-NIR-spectroscopic analysis of the resonance structures of Octenidine dihydrochloride

A second approach measured Octenidine dihydrochloride in solid state and in DMSO at different temperatures via near infrared spectroscopy (NIR). The measurements aimed to see, whether the verified dynamics observed in the NMR study are also discernible in the NIR spectra. NIR spectroscopic measurements allow a detailed study of the dynamics of the resonance from approx. 30 °C to 60 °C (303.15-333.15 K) for the Octenidine dihydrochloride in its solid-state. The measurements in DMSO were performed from 35 °C to 80 °C (308.15-353.15 K) (see Figure 5).

At first glance, in the spectra derived from the solid-state measurements, one area at approx. 5000 cm^{-1} can be detected (see Figure S39), where major differences between the samples at different temperatures, appear. The pretreatment was done with a Standard Normal Variate (SNV),[22] which is quite common to diminish the influence of physical properties of the samples (e.g. particle size). The identified area is part of the spectral region where combination bands can be found (especially: N–H; C–H and O–H).

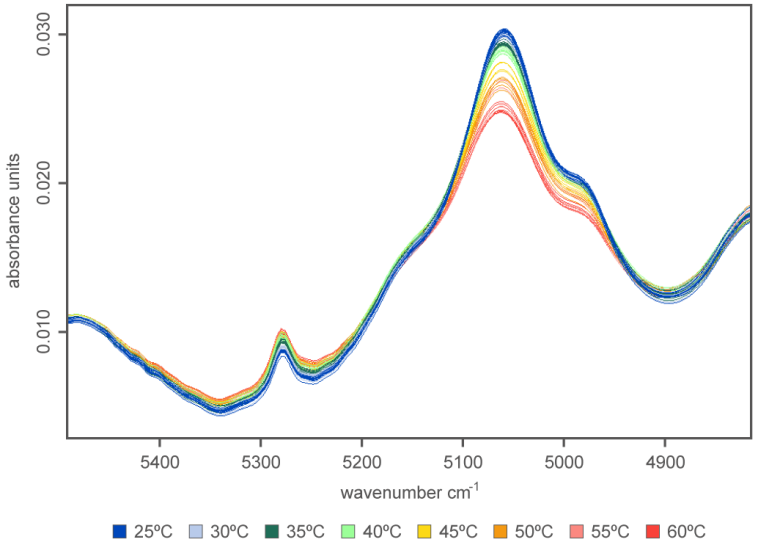

Figure 2. Pretreated NIR-spectra solid-state Octenidine dihydrochloride, SNV as pretreatment (Enlargement of the significant section).

The spectral range between 4820 and 5480 cm^{-1}, harbours two different peak areas (1.: 5250 to 5300 cm^{-1} and 2.: 4950 to 5100 cm^{-1}), which behave quite differently to each other. The first one is the typical region for the hydrogen bond in water (1. overtone in this case) and shows a relatively equal increase in absorbance relative to the temperature of the samples. The second region shows a differing behaviour due to a decrease in absorption especially around approx. 5032 cm^{-1}. In this region the N–H-bond-signal, which underlies certain molecular influences due to the mesomeric effect affecting the bond dipole moment, is expected. A visual comparison of the different spectra at 5032 cm^{-1} shows a disjointed decrease (especially in comparison to the H_2O-bond) of the absorbance indicating a structural change and not only the influence of temperature itself on the molecule. To prove this hypothesis a Principal Component Analysis (PCA) was performed with spectral data from 4980 to 5120 cm^{-1}. This is a common tool to analyse multivariate data in order to explore the variances in the set and to reduce the information particularly in co-correlated data sets (e.g. spectra). A spectrum with e.g. 1898 recorded data points represents an 1898-dimensional vector, which can be transcribed in a matrix row. This is done with the whole data set, allowing one to explore the data set in a vectorized space further on. The algorithm works by searching for the highest variance between the data (the so-called principal component 1) and optimizing the presentation of the data towards the highest variance(s). Secondly, a second principal component is searched in order to explain the remaining variance. And subsequently the remaining variance is being appointed to a principal component (defined maximum: 100 iterations). The variance left unexplained at the end of this iterative process represents residuals. The data was pretreated by SNV and secondly with a derivatization (second derivative, 17 smoothing points) by polynomial fitting according to Savitzky-Golay's procedure.[23]

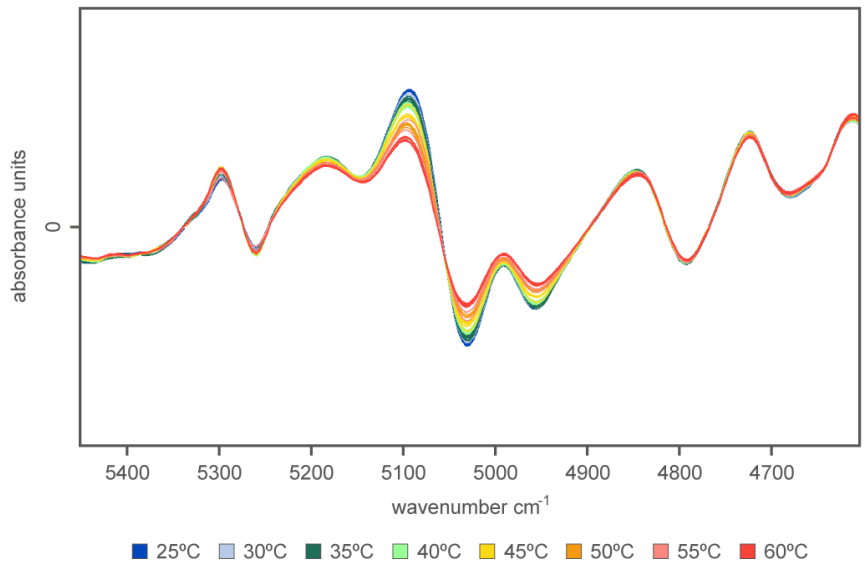

Figure 3. Pretreated NIR-spectra, solid-state Octenidine dihydrochloride (2. Derivative and SNV).

There are two reasons for this further pretreatment: On one hand the scattering correction by eliminating linear and multiplicative base line shifts and on the other hand the higher resolution of overlapping peaks. Thus, it was possible to define the spectral region impacted most by temperature changes.

As can be seen in Figure 4 there is a change occurring to the data beginning at 45-50 °C (approx. 318/323 K) and entering the next "phase" at 55 °C (approx. 328 K). In analogy to the NIR spectra, the results of 55 °C and 60 °C do not differ much. However, it proves in addition that there are non-linear changes in the absorbance measured at different temperatures, which indicate that a distinct resonance structure may occur. The dynamics already start changing around 45-50 °C resulting in the main occurrence of the resonance structure II at 55 °C (as shown with NMR).

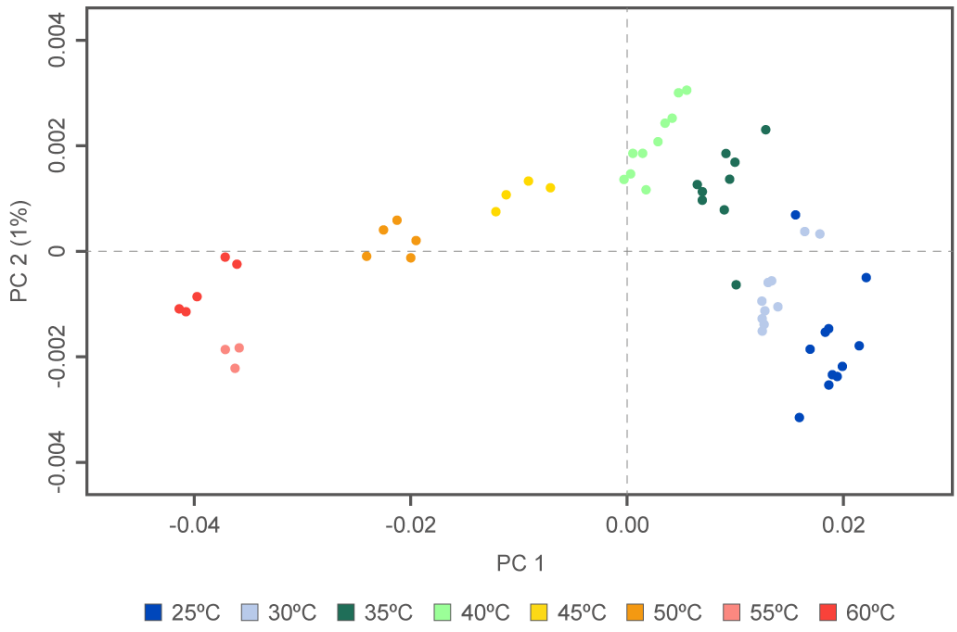

Figure 4. PCA-Plot: PC-1 vs. PC-2.

At higher temperatures the Octenidine dihydrochloride dissolved in DMSO shows a shift in the region of 5050 to 5100 cm^{-1} (see also Figure 5), which is probably the same as that observable in the solid-state spectra of Octenidine dihydrochloride. Comparing the behaviour to Octenidine-free DMSO itself (see Figure S43), it becomes clear that the temperature-dependent behaviour of DMSO itself cannot be the explanation for the shifts in this region. The sharp peak at ca. 5150 cm^{-1} displayed in the spectra of the samples with a temperature exceeding 55 °C, is also present in the DMSO spectra. Yet, in comparison to the Octenidine-solution this peak only changes its position slightly in DMSO-solution, but not its shape depending on the different temperatures. This is a characteristic feature of the Octenidine solution and provides an insight into the structural changes of the Octenidine dihydrochloride occurring at higher temperatures in the solution.

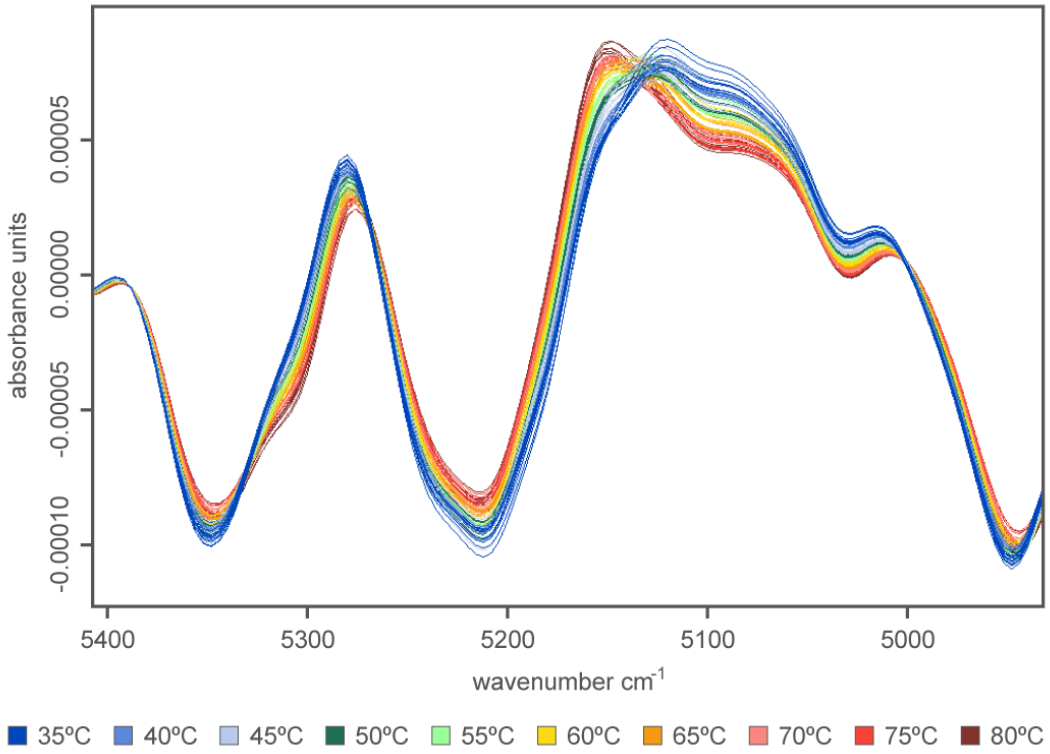

Figure 5. Pretreated NIR-spectra of Octenidine dihydrochloride in DMSO (1. Derivative and SNV).

Conclusions

Summarizing the results of NMR and NIR spectroscopy it can be stated that, especially NMR spectroscopy, is a very powerful tool to characterize an API like Octenidine dihydrochloride. Not only general characterization and structure elucidation could be performed with NMR, but also a study of the resonance dynamics was possible. A hindered rotation of the heteroaromatic could be identified using NMR spectroscopy. But the energy barrier is not that high. Nevertheless, the hindered rotation might have an effect on the mechanism of action with tissue material. The temperature-dependent changes can be shown using the NIR spectrometry. In this study, at 330-340 K (approx. 57-67 °C) the resonance structure **II** is more appropriate to explain the state of the Octenidine dihydrochloride. However, at 310 K (approx. 37 °C) the resonance structure **I** has also to be considered. This could be emphasized by the NIR study, showing in addition that it is possible to analyse the

spectral shift due to the different sample temperatures, being modified by the mesomeric effect with NIR spectroscopy. Both studies demonstrate the importance of analysing and understanding the molecular dynamics of the API, especially those effects which are easily detectable by NMR and NIR spectroscopy. A more detailed investigation of the dynamics of the aliphatic chain and the complete conformational space might be necessary, presumably only on a theoretical level. No apparent effects could be observed e.g. in the NMR spectra in the investigated temperature range for the aliphatic signals. The question remains, whether the adverse drug reactions of Octenidine dihydrochloride occurring when used in cavities and deep wounds can be linked to the temperature-dependent resonance structures, especially the quaternary pyridinium ion.[24] Further investigation of this topic is needed to provide further insights.

Experimental Section

NMR-spectroscopy. NMR spectra were measured either on a Bruker Avance III 300 spectrometer or a Bruker Avance III 400 NMR spectrometer (Bruker, Rheinstetten, Germany) equipped with a variable temperature unit, a standard probe head for the detection of proton and heteroatoms with deuterium lock (PABBO), gradient unit and automatic tuning and shimming. Temperature calibration was done with a solution of methanol-d_4. Either DMSO-d_6 (99.8%) or $CDCl_3$ was used (Eurisotop). For the measurements at 300 MHz a sample of 31 mg of Octenidine dihydrochloride in 0.6 mL of DMSO-d_6 and 150 mg in 0.6 mL of $CDCl_3$ was used, at 400 MHz the concentration was 12 mg in 0.6 mL of DMSO-d_6. The higher concentrated solution of Octenidine in DMSO-d_6 showed crystallization of the drug below 310 K, the solution of 12 mg of the drug was stable at 298 K, so standard 1D and 2D spectra were recorded at 400 MHz using the pulse programs of the manufacturer's pulse program library at this temperature. For the temperature dependent ^{1}H NMR spectra after reaching the measuring temperature the sample was allowed to equilibrate for a further 3 minutes, and for each temperature the probe head was automatically tuned and matched and the sample was reshimmed. For the temperature measurements in DMSO-d_6, a plot of the proton resonance shift of the water signal versus temperature gives an excellent linear fit (R^2 = 0.997) when using a calibration via the measuring frequency setting, indicating that equilibrium temperature was achieved in the sample for all spectra. NMR spectra were measured and calibrated to the internal standard or residual solvent signals, that is DMSO-d_5 ^{1}H (400 MHz): 2.50 ppm, TMS 0.00 ppm, DMSO-d_6 ^{13}C (100 MHz): 39.50 ppm, ^{15}N (30.4 MHz): spectra were referenced to external nitromethane in the corresponding solvent, measured in an HMBC experiment and set to 0.0 ppm. Details of recalculating different reference shifts for the ^{15}N nucleus are given in the supporting information and are partly taken from[25] and references therein.

Spectra were processed using Bruker TOPSPIN 3.6 with standard processing parameters for the respective type of 1D or 2D spectrum. The temperature dependent NMR spectra were recorded with 64 K data points and were processed with a Gauß multiplication and zero filling with a line broadening factor of –0.1 and a Gauß multiplication factor of 0.1. ^{13}C and ^{1}H NMR chemical shifts were predicted for the mesomeric forms in Figure 1 using the online portals of the CSEARCH program (^{13}C nucleus[26]) and the nmrdb.org website (^{1}H nucleus[27]). For the line shape analysis, the shift region in the range of 6.5 to 8.5 ppm was simulated and dynamic processes were investigated using Spinworks 4.2.9,[28] especially the DNMR3 calculation suite.[29] The results of the simulation were evaluated by the spectroscopist's eye and the exchange rate constants were determined. No further adjustments of the exchange rate constants were made after plotting in order to improve the correlation. The Eyring plot of ln(k/T) versus 1/T was performed conveniently on Arrhenius and Eyring calculations on Clymer's website.[30]

In the supporting information a visualization of possible conformations of the two mesomeric structures was achieved using OpenBabel 2.3.0 and AutoDockTools-1.5.4 via an internet portal[31] and presentation with Rasmol.[32] The Hückel MO charge distribution was calculated with Marvin Sketch 19.18.[33]

NIR-spectroscopy. The measurements were performed using a TANGO-R and a TANGO-T FT-NIR-spectrometer of Bruker Optics (Ettlingen, Germany). The solid Octenidine dihydrochloride was measured via diffuse reflection spectroscopy, while the Octenidine dihydrochloride containing DMSO-solution was measured in transmission (glass vials, 10 mm optical path length). The samples were tempered using a heating block (Accuracy according to manufacturer: -/+2 °C). The software used for the measurements was OPUS 7.5 (Bruker Optics, Ettlingen). For the purpose of analysis, the OPUS software was used as well as The Unscrambler X (CAMO Analytics, Oslo). The PCA was performed with the Unscrambler X-software using the NIPALS algorithm and the default parameters recommended by the software provider. All spectra were measured with 128 single scans and a spectral resolution of 8 cm^{-1}.

Supplementary Material

Supporting information for this article is given via a link in the document.

References

1. Schmidt, J.; Zyba, V.; Jung, K.; Rinke, S.; Haak, R.; Mausberg, R. F.; Ziebolz, D. *Drug Chem. Toxicol.* **2016**, *39*, 322–330. http://dx.doi.org/10.3109/01480545.2015.1121274
2. Schülke&Mayr GmbH, *Rote-Hand-Brief zu Octenisept®*, **2011**, Dr. Jörg Siebert.
3. Hübner, N. O.; Siebert, J.; Kramer, A. *Skin Pharmacol. Physiol.* **2010**, *23*, 244–258. http://dx.doi.org/10.1159/000314699
4. National Center for Biotechnology Information. PubChem Database. Cetylpyridinium chloride, CID=31239, https://pubchem.ncbi.nlm.nih.gov/compound/Cetylpyridinium-chloride (accessed 17 December 2019).
5. Roberts, W. R.; Addy, M. *J. Clin. Periodont.* **1981**, *8*, 295–310. https://doi.org/10.1111/j.1600-051X.1981.tb02040.x
6. Aires-de-Sousa, J.; Hemmer, M. C.; Gasteiger, J. *Anal. Chem.* **2002**, *74*, 80-90. https://doi.org/10.1021/ac010737m
7. Binev, Y.; Marques, M. M. B.; Aires-de-Sousa, J. *J. Chem. Inf. Model.* **2007**, *47*, 2089-2097. https://doi.org/10.1021/ci700172n
8. Schütz, V.; Purtuc, V.; Felsinger, S.; Robien, W. *Fresenius J. Anal. Chem.* **1997**, *359*, 33-41. https://doi.org/10.1007/s002160050531
9. Kuhn, S.; Johnson, S. R. *ACS Omega* **2019**, *4*, 7323-7329. https://doi.org/10.1021/acsomega.9b00488
10. Robien, W. *Monatsh. Chem*. **2019**, *150*, 927-932. https://doi.org/10.1007/s00706-019-02407-5
11. Beltrame, P.; Cadoni, E.; Floris, C.; Gelli, G.; Lai, A. *Spectrochim. Acta A* **2002**, *58*, 2693–2697. https://doi.org/10.1016/S1386-1425(02)00015-X

12. Dokalik, A.; Kalchhauser, H.; Mikenda, W.; Schweng, G. *Magn. Res. Chem.* **1999**, *37*, 895–902. https://doi.org/10.1002/(SICI)1097-458X(199912)37:12<895::AID-MRC581>3.0.CO;2-7
13. Sammes, M. P.; Lai, T. F.; Katrizky, A. R.; Murugan, R.; Luce, H. *J. Chem. Soc., Perkin Trans. 2* **1985**, 573–579. https://doi.org/10.1039/P29850000573
14. Semenov, V. A.; Samultsev, D. O.; Krivdin, L. B. *Magn. Res. Chem.* **2015**, *53*, 433–441. https://doi.org/10.1002/mrc.4231
15. Semenov, V. A.; Samultsev, D. O.; Krivdin, L. B. *Magn. Res. Chem.* **2018**, *56*, 727–739. https://doi.org/10.1002/mrc.4721
16. Muccio, D. D.; Copan, W. G.; Abrahamson, W. W.; Mateescu, G. D. *Org. Magn. Res.* **1984**, 22, 121–124. https://doi.org/10.1002/mrc.1270220214
17. Schilf, W.; Kamieński, B.; Szady-Chełmieniecka, A.; Grech, E. *J. Mol. Struct.* **2004**, 700, 105–108. https://doi.org/10.1016/j.molstruc.2003.12.052
18. Günther, H. *NMR spectroscopy*, 3rd Ed., Wiley-VCH: Weinheim, 2013; pp 501–518.
19. Eliel, E.L.; Wilen, S.H.; Mander, L.N. *Stereochemistry of Organic Compounds*, Wiley: New York, 1994; pp 550–554. https://doi.org/10.1002/9780470147306
20. Jennings, W. B.; Al-Showiman, S.; Tolley, M. S.; Boyd, D. R. *J. Chem. Soc., Perkin Trans. 2* **1975**, 1535–1539. https://doi.org/10.1039/P29750001535
21. Johnson, J. E.; Morales, N. M.; McAllister, M. A. *J. Org. Chem.* **2001**, 66, 7979–7985. https://doi.org/10.1021/jo010067k
22. Véstia, J.; Barroso, J. M.; Ferreira, H.; Gaspar, L.; Rato, A. E. *Food C hem.* **2019**, 276, 71-76. http://dx.doi.org/10.1016/j.foodchem.2018.09.116.
23. Rinnan, A.; van den Berg, F.; Engelsen, S. B. *TrAC Trends in Analytical Chemistry* **2009**, 28, 1201-1222. http://dx.doi.org/10.1016/j.trac.2009.07.007.
24. Hülsemann, W.; Habenicht, R. *Handchir. Mikrochir. Plast. Chir*. **2009**, 41, 277-282. http://dx.doi.org/10.1055/s-0029-1238282.
25. Martin, G.E.; SoIntseva, M.; Williams, A.J. In *Application of 15N NMR Spectroscopy in Alkaloid Chemistry, Modern Alkaloids*; E. Fattorusso, O. Taglialatela-Scafati Eds.; Wiley-VCH: Weinheim, 2008; pp 409–471.
26. Haider, N.; Robien, W. CSEARCH Robot Referee. http://nmrpredict.orc.univie.ac.at/c13robot/robot.php (accessed 01 July 2019).
27. Castillo, A. M.; Patiny M.; Wist, L. *J. Magn. Res.* **2011**, 209, 123–130; http://www.nmrdb.org/ (accessed 01 July 2019).
28. Marat, K. SpinWorks 4.2.9, (accessed 01 July 2019), University of Manitoba.
29. Stephenson, D. S.; Binsch, G. *J. Magn. Res.* **1978**, 30, 625–626.
30. Clymer, J. http://clymer.altervista.org/arr/ 2015, (accessed 01 July 2019).
31. Li, Q.; Xiang, J.-F.; Yang, Q.-F.; Sun, H.-X.; Guan, A.-J.; Tang, J.-L. *Nucl. Acids Res.*, **2013**, 41, D1115–D1123; www.gl4db.org (accessed 01 July 2019).
32. Rasmol, Windows Version 2.7.5.2., www.rasmol.org (accessed 01 July 2019).
33. MarvinSketch 18.19, Huckel analysis plugin evaluation mode, www.chemaxon.com (accessed 01 July 2019).